Technihadron Production and Decay in Low-Scale Technicolor

Kenneth Lane[*]

Department of Physics, Boston University

590 Commonwealth Avenue, Boston, MA 02215

February 7, 2008

Abstract

We discuss the production and decay rates of the lightest color-singlet technihadrons, spin-one ρ_T and ω_T and spin-zero π_T, in a minimal "straw-man" model of low-scale techicolor. The revised ρ_T and ω_T decay rates affect the technicolor searches planned for Run II of the Tevatron Collider.

arXiv:hep-ph/9903369v3   26 Mar 1999

[*]lane@buphyc.bu.edu

1 Introduction

Modern technicolor models of dynamical electroweak symmetry breaking require a walking technicolor gauge coupling [1] to evade large flavor-changing neutral current effect and the assistance of topcolor interactions that are strong near 1 TeV [2, 3, 4] to provide the large mass of the top quark. Both additions to the basic technicolor scenario [5, 6] tend to require a large number N_D of technifermion doublets. Many technifermions are needed to make the beta function of walking technicolor small. And many seem to be required in topcolor-assisted technicolor to generate the hard masses of quarks and leptons, to induce the correct mixing between heavy and light quarks, and to break topcolor symmetry down to ordinary color. As has been emphasized [7, 8], large N_D implies a relatively low technihadron mass scale, set by the technipion decay constant $F_T \simeq F_\pi / \sqrt{N_D}$, where $F_\pi = 246\,\mathrm{GeV}$. In the models of Ref. [4], for example, $N_D \simeq 10$ and $F_T \simeq 80\,\mathrm{GeV}$. It is likely that this low-scale technicolor will be within reach of the Tevatron Collider Run II experiments. [1] Indeed, preliminary searches based on Run I data have been carried out or are in progress for several of its color-singlet signals [9, 10, 11].

In this paper we re-examine the decay and production rates for color-singlet technivector mesons, $V_T = \rho_T$ and ω_T. Special attention is given to the decay $V_T \to G\pi_T$, where G is a transversely polarized electroweak gauge boson, γ, Z^0, $W^\pm$, and π_T is a technipion. The gauge boson polarization is defined relative to the spin direction of the technivector meson in the latter's rest frame. (This is the same as the beam direction in a hadron or lepton collider.) Some of these decay rates, particularly those involving a photon, can be as large as the modes previously considered [8]. If this happens, branching ratio expectations are different from Ref. [8] and the limits placed by analyses in Ref. [9, 10, 11] must be reinterpreted. In any case, signal rates are large enough that technicolor searches in Run II will severely restrict the expected parameter space of low-scale technicolor.

To set the ground rules for our calculations, we adopt the "Technicolor Straw Man Model". In the TCSM, we assume that we can consider in isolation the lowest-lying bound states of the lightest technifermion doublet, (T_U, T_D). These technifermions are likely to be color singlets because color-

---

[1]The Run II conditions assumed in this paper are $p\bar{p}$ collisions at center-of-mass energy $\sqrt{s} = 2\,\mathrm{TeV}$ for an integrated luminosity of $2\,\mathrm{fb}^{-1}$.

$SU(3)$ interactions contribute significantly to their hard mass [7]. We shall assume that they transform under technicolor $SU(N_{TC})$ as fundamentals. Their electric charges are Q_U and Q_D. The bound states in question are vector and pseudoscalar mesons. The vectors include a spin-one isotriplet $\rho_T^{\pm,0}$ and an isosinglet ω_T. In topcolor-assisted technicolor, there is no need to invoke large isospin-violating extended technicolor interactions to explain the top-bottom splitting. Thus, techni-isospin can be, and likely must be, a good approximate symmetry. Then, ρ_T and ω_T will be nearly degenerate. Their mixing will be described in the neutral-sector propagator matrix, Δ_0, in Eq. (18) below.

The lightest pseudoscalar (T_U, T_D) bound states, the technipions, also comprise an isotriplet $\Pi_T^{\pm,0}$ and an isosinglet $\Pi_T^{0\prime}$. However, these are not mass eigenstates. In the TCSM, we assume the isovectors are simple two-state mixtures of the longitudinal weak bosons $W_L^{\pm}$, Z_L^0—the true Goldstone bosons of dynamical electroweak symmetry breaking in the limit that the $SU(2) \otimes U(1)$ couplings g, g' vanish—and mass-eigenstate pseudo-Goldstone technipions $\pi_T^{\pm}, \pi_T^0$:

$$|\Pi_T\rangle = \sin\chi\,|W_L\rangle + \cos\chi\,|\pi_T\rangle. \qquad (1)$$

Here, $\sin\chi = F_T/F_\pi \ll 1$.

Similarly, $|\Pi_T^{0\prime}\rangle = \cos\chi\,'\,|\pi_T^{0\prime}\rangle + \cdots$, where χ' is another mixing angle and the ellipsis refer to other technipions needed to eliminate the two-technigluon anomaly from the $\Pi_T^{0\prime}$ chiral current. It is unclear whether, like ρ_T and ω_T, these neutral technipions will be degenerate as we have previously supposed [8]. On one hand, they both contain the lightest $\bar{T}T$ as constituents. On the other, $\pi_T^{0\prime}$ must contain other, presumably heavier, technifermions as a consequence of anomaly cancellation. In our calculations, we shall assume as before that π_T^0 and $\pi_T^{0\prime}$ are nearly degenerate. We reiterate the point made in Ref. [8] that, if they are and if their widths are roughly equal, there will be appreciable π_T^0–$\pi_T^{0\prime}$ mixing. Then, the lightest neutral technipions will be ideally-mixed $\bar{T}_U T_U$ and $\bar{T}_D T_D$ bound states. In any case, the technipions are expected to decay as follows: $\pi_T^+ \to c\bar{b}$ or $c\bar{s}$ or even $\tau^+\nu_\tau$; $\pi_T^0 \to b\bar{b}$ and, perhaps $c\bar{c}$, $\tau^+\tau^-$; and $\pi_T^{0\prime} \to gg$, $b\bar{b}$, $c\bar{c}$, $\tau^+\tau^-$. [2]

---

[2]All technihadron decay and production rates in the TCSM are compiled for easy reference in a companion to this paper, Ref. [12].

In the limit that the electroweak couplings $g, g' = 0$, the ρ_T and ω_T decay as

$$\rho_T \rightarrow \Pi_T \Pi_T = \cos^2 \chi \, (\pi_T \pi_T) + 2 \sin \chi \, \cos \chi \, (W_L \pi_T) + \sin^2 \chi \, (W_L W_L) \, ;$$

$$\omega_T \rightarrow \Pi_T \Pi_T \Pi_T = \cos^3 \chi \, (\pi_T \pi_T \pi_T) + \cdots . \tag{2}$$

The ρ_T decay amplitude is

$$\mathcal{M}(\rho_T(q) \rightarrow \pi_A(p_1)\pi_B(p_2)) = g_{\rho_T} \mathcal{C}_{AB} \, \epsilon(q) \cdot (p_1 - p_2) \, , \tag{3}$$

where $\epsilon(q)$ is the ρ_T polarization vector; $\alpha_{\rho_T} \equiv g_{\rho_T}^2/4\pi = 2.91(3/N_{TC})$ is scaled naively from QCD and $N_{TC} = 4$ is used in calculations; and

$$\mathcal{C}_{AB} = \begin{cases} \sin^2 \chi & \text{for } W_L^+ W_L^- \text{ or } W_L^\pm Z_L^0 \\ \sin \chi \cos \chi & \text{for } W_L^+ \pi_T^-, W_L^- \pi_T^+ \text{ or } W_L^\pm \pi_T^0, Z_L^0 \pi_T^\pm \\ \cos^2 \chi & \text{for } \pi_T^+ \pi_T^- \text{ or } \pi_T^\pm \pi_T^0 \, . \end{cases} \tag{4}$$

The ρ_T decay rate to two technipions is then (for later use in cross sections, we quote the energy-dependent width for a ρ_T mass of $\sqrt{\hat{s}}$)

$$\Gamma(\rho_T^0 \rightarrow \pi_A^+ \pi_B^-) = \Gamma(\rho_T^\pm \rightarrow \pi_A^\pm \pi_B^0) = \frac{2\alpha_{\rho_T} \mathcal{C}_{AB}^2}{3} \frac{p^3}{\hat{s}} \, , \tag{5}$$

where $p = [(\hat{s} - (M_A + M_B)^2)(\hat{s} - (M_A - M_B)^2)]^{\frac{1}{2}}/2\sqrt{\hat{s}}$ is the π_T momentum in the ρ_T rest frame.

Now, walking technicolor enhancements of technipion masses are likely to close off the channels $\rho_T \rightarrow \pi_T \pi_T$, $\omega_T \rightarrow \pi_T \pi_T \pi_T$ and even the isospin-violating $\omega_T \rightarrow \pi_T \pi_T$ [7]. A technirho of, say, 200 GeV may then decay to $W_L \pi_T$ or $W_L W_L$, but how does a light techniomega decay? The answer is that all its decays are electroweak, $\omega_T \rightarrow \gamma \pi_T^0$, $Z^0 \pi_T^0$, $W^\pm \pi_T^\mp$, etc., where Z and W may be either transversely or longitudinally polarized. This raises the further question: Since $\sin^2 \chi \ll 1$, the electroweak decays of ρ_T to the transverse gauge bosons γ, W, Z plus a technipion may be competitive with the open-channel strong decays. How do we correctly describe these $g, g' \neq 0$ transitions? If the rates for these radiative decays are not negligible, they affect expectations for the existing and planned searches for $\rho_T \rightarrow W \pi_T$, $\omega_T \rightarrow \gamma \pi_T^0$ and $\rho_T, \omega_T \rightarrow f_i \bar{f}_i$.

4

In Section 2, we discuss the form of the amplitudes for the decays $V_T \to G\pi_T$ where $G = \gamma, Z^0, W^{\pm}$ is transversely polarized. We shall see that, depending on the size of technicolor-scale mass parameters $M_{V,A}$ and technifermion charges $Q_{U,D}$, several of these decays have rates as large as those considered in Ref. [8]. In Section 3, we present the cross sections for all $q\bar{q} \to \rho_T, \omega_T \to X$ subprocesses of interest in the color-singlet sector of the TCSM. Section 4 contains a sample of numerical results for ρ_T and ω_T signal rates in $p\bar{p}$ collisions at $\sqrt{s} = 2\,\text{TeV}$.

2 $\quad \rho_T, \omega_T \to \gamma/W/Z + \pi_T$ when $g, g' \neq 0$

It is simplest to start with the decay $\omega_T \to \gamma\pi_T^0$ considered already in Ref. [8]. Gauge invariance, chiral symmetry, angular momentum and parity conservation imply that the lowest-dimensional operator mediating this decay is $(e/M_V)\, F_{\rho_T} \cdot \widetilde{F}_\gamma\, \pi_T^0$ where, naively scaling from analogous decays in QCD, M_V is a parameter of order several 100 GeV. [3] To fix its normalization, we write this decay amplitude as

$$\mathcal{M}(\omega_T(q) \to \gamma(p_1)\pi_T^0(p_2)) = \frac{e\cos\chi}{M_V}\epsilon^{\mu\nu\lambda\rho}\epsilon_\mu(q)\epsilon_\nu^*(p_1)q_\lambda p_{1\rho}\,. \tag{6}$$

It is now clear on dynamical and symmetry grounds that the amplitude for decay to any transversely polarized electroweak boson G plus a technipion can be written as

$$
\begin{aligned}
\mathcal{M}(V_T(q) \to G(p_1)\pi_T(p_2)) &= \frac{eV_{V_T G\pi_T}}{M_V}\,\epsilon^{\mu\nu\lambda\rho}\,\epsilon_\mu(q)\,\epsilon_\nu^*(p_1)\,q_\lambda\,p_{1\rho} \tag{7}\\
&+ \frac{eA_{V_T G\pi_T}}{M_A}\Big(\epsilon(q)\cdot\epsilon^*(p_1)\,q\cdot p_1 - \epsilon(q)\cdot p_1\,\epsilon^*(p_1)\cdot q\Big)\,.
\end{aligned}
$$

The first term corresponds to the vector coupling of G to the constituent technifermions of V_T and π_T and the second term to its axial-vector coupling. Note that the amplitudes for emission of longitudinally polarized bosons in Eq. (3) and transversely polarized ones in Eq. (7) are noninterfering, as they should be. On dynamical grounds, the mass parameter M_A is expected to be comparable to M_V. If we adopt a "valence technifermion" model for the

---

[3]The corresponding $\rho \to \gamma\pi$ parameter in QCD is about 400 MeV. A large–N_c argument implies $M_V \simeq (F_T/f_\pi)\,400\,\text{MeV} \simeq 350\,\text{GeV}$.

graphs describing Eq. (7)—a model which works very well for $\omega, \rho \to \gamma\pi$ and $\gamma\eta$ in QCD—CP-invariance implies that the V and A coefficients in this amplitude are given in our normalization by [4]

$$V_{V_T G \pi_T} = \text{Tr}\left(Q_{V_T}\{Q_{G_V}^\dagger, Q_{\pi_T}^\dagger\}\right), \qquad A_{V_T G \pi_T} = \text{Tr}\left(Q_{V_T}[Q_{G_A}^\dagger, Q_{\pi_T}^\dagger]\right). \quad (8)$$

In the TCSM, with electric charges Q_U, Q_D for T_U, T_D, the generators Q in Eq. (8) are given by

$$
\begin{aligned}
Q_{\rho_T^0} &= \frac{1}{\sqrt{2}}\begin{pmatrix} 1 & 0 \\ 0 & -1 \end{pmatrix}; \qquad Q_{\rho_T^+} = Q_{\rho_T^-}^\dagger = \begin{pmatrix} 0 & 1 \\ 0 & 0 \end{pmatrix} \\
Q_{\pi_T^0} &= \frac{\cos\chi}{\sqrt{2}}\begin{pmatrix} 1 & 0 \\ 0 & -1 \end{pmatrix}; \quad Q_{\pi_T^+} = Q_{\pi_T^-}^\dagger = \cos\chi\begin{pmatrix} 0 & 1 \\ 0 & 0 \end{pmatrix} \\
Q_{\pi_T^{0\prime}} &= \frac{\cos\chi'}{\sqrt{2}}\begin{pmatrix} 1 & 0 \\ 0 & 1 \end{pmatrix} \\
Q_{\gamma_V} &= \begin{pmatrix} Q_U & 0 \\ 0 & Q_D \end{pmatrix}; \qquad Q_{\gamma_A} = 0 \\
Q_{Z_V} &= \frac{1}{\sin\theta_W \cos\theta_W}\begin{pmatrix} \frac{1}{4} - Q_U \sin^2\theta_W & 0 \\ 0 & -\frac{1}{4} - Q_D \sin^2\theta_W \end{pmatrix} \\
Q_{Z_A} &= \frac{1}{\sin\theta_W \cos\theta_W}\begin{pmatrix} -\frac{1}{4} & 0 \\ 0 & \frac{1}{4} \end{pmatrix} \\
Q_{W_V^+} &= Q_{W_V^-}^\dagger = -Q_{W_A^+} = -Q_{W_A^-}^\dagger = \frac{1}{2\sqrt{2}\sin\theta_W}\begin{pmatrix} 0 & 1 \\ 0 & 0 \end{pmatrix} \qquad (9)
\end{aligned}
$$

The decay rate for $V_T \to G \pi_T$ is

$$\Gamma(V_T \to G \pi_T) = \frac{\alpha V_{V_T G \pi_T}^2 \, p^3}{3M_V^2} + \frac{\alpha A_{V_T G \pi_T}^2 \, p\,(3M_G^2 + 2p^2)}{6M_A^2}, \qquad (10)$$

where p is the G-momentum in the V_T rest frame. The V and A coefficients and sample decay rates are listed in Table 1. These are to be compared with the rates for decay into longitudinal W and Z bosons plus a technipion

---

[4] We have neglected decays such as $\rho_T^0 \to W_T W_L$ and $\rho_T^0 \to W_T W_T$. The rate for the former is suppressed by $\tan^2\chi$ relative to the rate for $\rho_T^0 \to W_T \pi_T$ while the latter's rate is suppressed by α.

quoted in Ref. [8]. For $M_{\rho_T} = 210\,\mathrm{GeV}$, $M_{\pi_T} = 110\,\mathrm{GeV}$, and $N_{TC} = 4$, they are

$$\begin{aligned}
\Gamma(\rho_T^0 \to W_L^\pm \pi_T^\mp) &= \Gamma(\rho_T^\pm \to W_L^\pm \pi_T^0) = 2.78 \sin^2\chi \cos^2\chi \\
\Gamma(\rho_T^\pm \to Z_L^0 \pi_T^\mp) &= 0.89 \sin^2\chi \cos^2\chi\,.
\end{aligned} \tag{11}$$

For $\sin^2\chi = 1/9$, our nominal choice, and for $M_V = M_A = 100\,\mathrm{GeV}$, the rates for ρ_T and $\omega_T \to \gamma\pi_T$ and for $\rho_T \to W_T\pi_T$, $Z_T\pi_T$ via axial vector coupling are comparable to these. Obviously, these transverse-boson decay rates fall quickly for greater M_V and M_A.

We can estimate the rate for the isospin-violating decay $\omega_T \to W_T^\pm \pi_T^\mp$ as

$$\Gamma(\omega_T \to W_L^\pm \pi_T^\mp) = |\epsilon_{\rho\omega}|^2\, \Gamma(\rho_T^0 \to W_L^\pm \pi_T^\mp)\,, \tag{12}$$

where $\epsilon_{\rho\omega}$ is the ρ_T-ω_T mixing amplitude. In QCD, $|\epsilon_{\rho\omega}| \simeq 5\%$, so we expect this decay mode to be entirely negligible.

Finally, for completeness, we record here the decay rates for $\rho_T, \omega_T \to f\bar{f}$. The ρ_T decay rates to fermions with $N_f = 1$ or 3 colors are [5]

$$\Gamma(\rho_T^0 \to f_i \bar{f}_i) = \frac{N_f \alpha^2 p}{3\alpha_{\rho_T} \hat{s}} \left((\hat{s} - m_i^2)\, A_i^0(\hat{s}) + 6m_i^2\, \mathcal{R}e(\mathcal{A}_{iL}(\hat{s})\mathcal{A}_{iR}^*(\hat{s})) \right)\,, \tag{13}$$

$$\Gamma(\rho_T^+ \to f_i \bar{f}_i') = \frac{N_f \alpha^2 p}{6\alpha_{\rho_T} \hat{s}^2} \left(2\hat{s}^2 - \hat{s}(m_i^2 + m_i'^2) - (m_i^2 - m_i'^2)^2 \right) A_i^+(\hat{s})\,,$$

where a unit CKM matrix is assumed in the second equality. The quantities A_i are given by

$$A_i^\pm(\hat{s}) = \frac{1}{8\sin^4\theta_W} \left| \frac{\hat{s}}{\hat{s} - \mathcal{M}_W^2} \right|^2\,,$$

$$A_i^0(\hat{s}) = |\mathcal{A}_{iL}(\hat{s})|^2 + |\mathcal{A}_{iR}(\hat{s})|^2\,, \tag{14}$$

---

[5]Eqs. (13), (14) and (16) below correct Eqs. (3) and (6) in the second paper and Eqs. (3) and (5) in the third paper of Ref. [8]. A factor of $M_{V_T}^4/\hat{s}^2$ that appears in Eqs. (6) and (11) of that second paper has been eliminated from Eqs. (13) and (16). This convention is consistent with the off-diagonal sf_{GV_T} terms in the propagator matrices $\Delta_{0,\pm}$ defined in Eqs. (18) and (20) below. For weakly-coupled narrow resonances such as ρ_T and ω_T, the difference is numerically insignificant.

where, for $\lambda = L, R$,

$$
\begin{aligned}
\mathcal{A}_{i\lambda}(\hat{s}) &= Q_i + \frac{2\zeta_{i\lambda} \cot 2\theta_W}{\sin 2\theta_W} \left(\frac{\hat{s}}{\hat{s} - \mathcal{M}_Z^2} \right), \\
\zeta_{iL} &= T_{3i} - Q_i \sin^2 \theta_W, \\
\zeta_{iR} &= -Q_i \sin^2 \theta_W.
\end{aligned}
\tag{15}
$$

Here, Q_i and $T_{3i} = \pm 1/2$ are the electric charge and left-handed weak isospin of fermion f_i. Also, $\mathcal{M}_{W,Z}^2 = M_{W,Z}^2 - i\sqrt{\hat{s}}\,\Gamma_{W,Z}(\hat{s})$, where $\Gamma_{W,Z}(\hat{s})$ is the weak boson's energy-dependent width. [6].

The ω_T decay rates to fermions with N_f colors are given by

$$
\Gamma(\omega_T \to \bar{f}_i f_i) = \frac{N_f \, \alpha^2 p}{3\alpha_{\rho_T}\hat{s}} \left((\hat{s} - m_i^2)\, B_i^0(\hat{s}) + 6m_i^2 \, \mathcal{R}e(\mathcal{B}_{iL}(\hat{s})\mathcal{B}_{iR}^*(\hat{s})) \right), \tag{16}
$$

where

$$
B_i^0(\hat{s}) = |\mathcal{B}_{iL}(\hat{s})|^2 + |\mathcal{B}_{iR}(\hat{s})|^2,
$$

$$
\mathcal{B}_{i\lambda}(\hat{s}) = \left[Q_i - \frac{4\zeta_{i\lambda} \sin^2 \theta_W}{\sin^2 2\theta_W} \left(\frac{\hat{s}}{\hat{s} - \mathcal{M}_Z^2} \right) \right] (Q_U + Q_D). \tag{17}
$$

3   Cross Sections

In this section we record cross sections for the hadron collider subprocesses $q\bar{q} \to V_T \to \pi_T\pi_T$, $G\pi_T$, and $f\bar{f}$. All of these these may be influenced by the fact that the $\rho_T \to \gamma\pi_T$ decay rates are comparable to the previously considered $\omega_T \to \gamma\pi_T^0$. Thus, for example, so long as ρ_T and ω_T are nearly degenerate and the technipions in question decay to at least one b-quark, these additional modes contribute to the signal of a photon plus dijets with a single b-tag studied in one recent CDF analysis [10].

As we'll see in the sample calculations in Section 4, it is important to include ρ_T-ω_T interference in these cross sections (also see the third paper

---

[6]Note, for example, that $\Gamma_Z(\hat{s})$ includes a $t\bar{t}$ contribution when $\hat{s} > 4m_t^2$.

Process	$V_{V_T G \pi_T}$	$A_{V_T G \pi_T}$	$\Gamma(V_T \to G_V \pi_T)$	$\Gamma(V_T \to G_A \pi_T)$
$\omega_T \to \gamma \pi_T^0$	c_χ	0	$0.115\ c_\chi^2$	0
$\to \gamma \pi_T^{0\prime}$	$(Q_U + Q_D)\, c_{\chi\prime}$	0	$0.320\ c_{\chi\prime}^2$	0
$\to Z^0 \pi_T^0$	$c_\chi \cot 2\theta_W$	0	$2.9 \times 10^{-3} c_\chi^2$	0
$\to Z^0 \pi_T^{0\prime}$	$-(Q_U + Q_D)\, c_{\chi\prime} \tan \theta_W$	0	$5.9 \times 10^{-3} c_{\chi\prime}^2$	0
$\to W^\pm \pi_T^\mp$	$c_\chi/(2 \sin \theta_W)$	0	$2.4 \times 10^{-2} c_\chi^2$	0
$\rho_T^0 \to \gamma \pi_T^0$	$(Q_U + Q_D)\, c_\chi$	0	$0.320\ c_\chi^2$	0
$\to \gamma \pi_T^{0\prime}$	$c_{\chi\prime}$	0	$0.115\ c_{\chi\prime}^2$	0
$\to Z^0 \pi_T^0$	$-(Q_U + Q_D)\, c_\chi \tan \theta_W$	0	$5.9 \times 10^{-3} c_\chi^2$	0
$\to Z^0 \pi_T^{0\prime}$	$c_{\chi\prime} \cot 2\theta_W$	0	$2.9 \times 10^{-3} c_{\chi\prime}^2$	0
$\to W^\pm \pi_T^\mp$	0	$-c_\chi/(2 \sin \theta_W)$	0	$0.143\ c_\chi^2$
$\rho_T^\pm \to \gamma \pi_T^\pm$	$(Q_U + Q_D)\, c_\chi$	0	$0.320\ c_\chi^2$	0
$\to Z^0 \pi_T^\pm$	$-(Q_U + Q_D)\, c_\chi \tan \theta_W$	$c_\chi / \sin 2\theta_W$	$5.9 \times 10^{-3} c_\chi^2$	$0.147\ c_\chi^2$
$\to W^\pm \pi_T^0$	0	$c_\chi/(2 \sin \theta_W)$	0	$0.143\ c_\chi^2$
$\to W^\pm \pi_T^{0\prime}$	$c_{\chi\prime}/(2 \sin \theta_W)$	0	$2.4 \times 10^{-2} c_{\chi\prime}^2$	0

Table 1: Amplitudes and sample decay rates (in GeV) for $V_T \to G\pi_T$. In the rate calculations, $M_{V_T} = 210\,\text{GeV}$, $M_{\pi_T} = 110\,\text{GeV}$, $M_V = M_A = 100\,\text{GeV}$; technifermion charges are $Q_U + Q_D = \frac{5}{3}$; $c_\chi = \cos \chi$ and $c_{\chi\prime} = \cos \chi\prime$; G_V and G_A refer to decays involving the vector and axial-vector couplings, respectively.

in Ref. [8]). In the TCSM, the γ–Z^0–ρ_T^0–ω_T propagator matrix Δ_0 is the inverse of

$$\Delta_0^{-1}(s) = \begin{pmatrix} s & 0 & -sf_{\gamma\rho_T} & -sf_{\gamma\omega_T} \\ 0 & s - \mathcal{M}_Z^2 & -sf_{Z\rho_T} & -sf_{Z\omega_T} \\ -sf_{\gamma\rho_T} & -sf_{Z\rho_T} & s - \mathcal{M}_{\rho_T^0}^2 & 0 \\ -sf_{\gamma\omega_T} & -sf_{Z\omega_T} & 0 & s - \mathcal{M}_{\omega_T}^2 \end{pmatrix}. \tag{18}$$

Note that, in the spirit of vector-meson dominance, we are assuming only kinetic mixing between the gauge bosons and technivector mesons. As noted earlier, whether this should be sf_{GV_T} or $M_{V_T}^2 f_{GV_T}$ is numerically irrelevant for narrow resonances. In setting the off-diagonal ρ_T^0–ω_T elemements of this matrix equal zero, we are guided by the smallness of this mixing in QCD and by the desire to keep the number of adjustable parameters in the TCSM as small as possible. Of course, such mixing can always be added if warranted. The properly normalized GV_T couplings are

$$f_{GV_T} = \sqrt{2}\,\xi\,\mathrm{Tr}\!\left(Q_{G_V} Q_{V_T}^\dagger\right); \tag{19}$$

in particular, $f_{\gamma\rho_T} = \xi$, $f_{\gamma\omega_T} = \xi\,(Q_U + Q_D)$, $f_{Z\rho_T} = \xi \cot 2\theta_W$, and $f_{Z\omega_T} = -\xi\,(Q_U + Q_D)\tan\theta_W$, where $\xi = \sqrt{\alpha/\alpha_{\rho_T}}$. In the charged sector, the $W^\pm$–$\rho_T^\pm$ matrix is the inverse of

$$\Delta_\pm^{-1}(s) = \begin{pmatrix} s - \mathcal{M}_W^2 & -sf_{W\rho_T} \\ -sf_{W\rho_T} & s - \mathcal{M}_{\rho_T^\pm}^2 \end{pmatrix}, \tag{20}$$

where $f_{W\rho_T} = \xi/(2\sin\theta_W)$.

The rates for production of any technipion pair, $\pi_A\pi_B = W_L W_L$, $W_L\pi_T$, and $\pi_T\pi_T$, in the isovector (ρ_T) channel are:

$$\frac{d\hat\sigma(q_i\bar q_i \to \rho_T^0 \to \pi_A^+\pi_B^-)}{d\hat t} =$$
$$\frac{\pi\alpha\alpha_{\rho_T}\mathcal{C}_{AB}^2(4\hat s p^2 - (\hat t - \hat u)^2)}{12\hat s^2}\left(|\mathcal{F}_{iL}^{\rho_T}(\hat s)|^2 + |\mathcal{F}_{iR}^{\rho_T}(\hat s)|^2\right), \tag{21}$$

and

$$\frac{d\hat\sigma(u_i\bar d_i \to \rho_T^+ \to \pi_A^+\pi_B^0)}{d\hat t} = \frac{\pi\alpha\alpha_{\rho_T}\mathcal{C}_{AB}^2(4\hat s p^2 - (\hat t - \hat u)^2)}{24\sin^2\theta_W\hat s^2}|\Delta_{W\rho_T}(\hat s)|^2, \tag{22}$$

10

where $p = [(\hat{s} - (M_A + M_B)^2)(\hat{s} - (M_A - M_B)^2)]^{\frac{1}{2}}/2\sqrt{\hat{s}}$ is the $\hat{s}$-dependendent momentum of $\pi_{A,B}$. As usual, $\hat{t} = M_A^2 - \sqrt{\hat{s}}(E_A - p\cos\theta)$, $\hat{u} = M_A^2 - \sqrt{\hat{s}}(E_A + p\cos\theta)$, where θ is the c.m. production angle of π_A. The factor $4\hat{s}p^2 - (\hat{t} - \hat{u})^2 = 4\hat{s}p^2\sin^2\theta$. The quantities $\mathcal{F}_{i\lambda}^{V_T}$ for $\lambda = L, R$ in Eq. (21) are given in terms of elements of Δ_0 by

$$\mathcal{F}_{i\lambda}^{V_T}(\hat{s}) = Q_i\,\Delta_{\gamma V_T}(\hat{s}) + \frac{2\zeta_{i\lambda}}{\sin 2\theta_W}\Delta_{ZV_T}(\hat{s})\,. \tag{23}$$

Because the ρ_T-ω_T mixing parameter $\epsilon_{\rho\omega}$ is expected to be very small, the rates for $q_i\bar{q}_i \rightarrow \omega_T \rightarrow \pi_A^+\pi_B^-$ are ignored here.

The cross section for $G\pi_T$ production in the neutral channel is given by

$$\frac{d\hat{\sigma}(q_i\bar{q}_i \rightarrow \rho_T^0,\,\omega_T \rightarrow G\pi_T)}{d\hat{t}} =$$
$$\frac{\pi\alpha^2}{24\hat{s}}\Bigg\{\left(|\mathcal{G}_{iL}^{VG\pi_T}(\hat{s})|^2 + |\mathcal{G}_{iR}^{VG\pi_T}(\hat{s})|^2\right)\left(\frac{\hat{t}^2 + \hat{u}^2 - 2M_G^2 M_{\pi_T}^2}{M_V^2}\right) \tag{24}$$
$$+ \left(|\mathcal{G}_{iL}^{AG\pi_T}(\hat{s})|^2 + |\mathcal{G}_{iR}^{AG\pi_T}(\hat{s})|^2\right)\left(\frac{\hat{t}^2 + \hat{u}^2 - 2M_G^2 M_{\pi_T}^2 + 4\hat{s}M_G^2}{M_A^2}\right)\Bigg\},$$

where, for $X = V, A$ and $\lambda = L, R$,

$$\mathcal{G}_{i\lambda}^{XG\pi_T} = \sum_{V_T = \rho_T^0,\omega_T} X_{V_T G\pi_T}\mathcal{F}_{i\lambda}^{V_T}\,. \tag{25}$$

The factor $\hat{t}^2 + \hat{u}^2 - 2M_G^2 M_{\pi_T}^2 = 2\hat{s}p^2(1 + \cos^2\theta)$. The $G\pi_T$ cross section in the charged channel is given by (in the approximation of a unit CKM matrix)

$$\frac{d\hat{\sigma}(u_i\bar{d}_i \rightarrow \rho_T^+ \rightarrow G\pi_T)}{d\hat{t}} = \frac{\pi\alpha^2}{48\sin^2\theta_W\,\hat{s}}\,|\Delta_{W\rho_T}(\hat{s})|^2 \tag{26}$$
$$\times\Bigg\{\frac{V_{\rho_T^+ G\pi_T}^2}{M_V^2}\left(\hat{t}^2 + \hat{u}^2 - 2M_G^2 M_{\pi_T}^2\right) + \frac{A_{\rho_T^+ G\pi_T}^2}{M_A^2}\left(\hat{t}^2 + \hat{u}^2 - 2M_G^2 M_{\pi_T}^2 + 4\hat{s}M_G^2\right)\Bigg\}\,.$$

The cross section for $q_i\bar{q}_i \rightarrow f_j\bar{f}_j$ (with $m_{q_i} = 0$ and allowing $m_{f_j} \neq 0$ for $t\bar{t}$ production) is

$$\frac{d\hat{\sigma}(q_i\bar{q}_i \rightarrow \gamma,\,Z \rightarrow \bar{f}_j f_j)}{d\hat{t}} = \frac{N_f\pi\alpha^2}{3\hat{s}^2}\Bigg\{\left((\hat{u} - m_{f_j}^2)^2 + m_{f_j}^2\hat{s}\right)\left(|\mathcal{D}_{ijLL}|^2 + |\mathcal{D}_{ijRR}|^2\right)$$
$$+ \left((\hat{t} - m_{f_j}^2)^2 + m_{f_j}^2\hat{s}\right)\left(|\mathcal{D}_{ijLR}|^2 + |\mathcal{D}_{ijRL}|^2\right)\Bigg\}, \tag{27}$$

11

where

$$\mathcal{D}_{ij\lambda\lambda'}(\hat{s}) = Q_i Q_j \, \Delta_{\gamma\gamma}(\hat{s}) + \frac{4}{\sin^2 2\theta_W} \, \zeta_{i\lambda} \, \zeta_{\text{J}\lambda'} \, \Delta_{ZZ}(\hat{s}) \qquad (28)$$

$$+ \frac{2}{\sin 2\theta_W} \left(\zeta_{i\lambda} Q_j \Delta_{Z\gamma}(\hat{s}) + Q_i \zeta_{j\lambda'} \Delta_{\gamma Z}(\hat{s}) \right).$$

Finally, the rate for the subprocess $u_i \bar{d}_i \to f_j \bar{f}'_j$ is

$$\frac{d\hat{\sigma}(u_i \bar{d}_i \to W^+ \to f_j \bar{f}'_j)}{d\hat{t}} = \frac{N_f \pi \alpha^2}{12 \sin^4 \theta_W \, \hat{s}^2} \, (\hat{u} - m_j^2)(\hat{u} - m_j'^2) \, |\Delta_{WW}(\hat{s})|^2 . \quad (29)$$

4   TCSM Signal Rates at the Tevatron

We present here a sampling of decay and production rates at the Tevatron for $M_{\rho_T} = 210\,\text{GeV}$, $M_{\omega_T} = 200\text{--}220\,\text{GeV}$, $M_{\pi_T} = M_{\pi_T^{0'}} = 110$ and $100\,\text{GeV}$, and $M_V = M_A = 100\text{--}500\,\text{GeV}$. We consider two plausibly extreme cases for the technifermion charges, $Q_U + Q_D = 5/3$ and $Q_U + Q_D = 0$, where $Q_D = Q_U - 1$. In the latter case ρ_T and ω_T decays to $\pi_T + \gamma$ are suppressed and $\omega_T \to f\bar{f}$ decays are forbidden altogether. In all calculations, $N_{TC} = 4$ and $\sin\chi = \sin\chi' = 1/3$. Since these calculations are at the parton level, they should be regarded as a rough guide to what can be expected. Detailed simulations are being carried out by Mrenna and Womersley [13], who have encoded the TCSM production and decay processes into the PYTHIA event generator [14] and incorporated the effects of a model detector appropriate to Run II conditions.

Case 1: $M_{\pi_T} = 110\,\text{GeV}$; $Q_U + Q_D = 5/3$

The total ρ_T and ω_T decay rates are plotted versus M_V in Fig. 1. The dominant decay modes of ρ_T^0 and $\rho_T^\pm$ are $W\pi_T$ and $\gamma\pi_T$. The rates to these two modes are roughly equal at $M_V = M_A = 100\,\text{GeV}$, but the $\gamma\pi_T$ rate falls off as M_V^{-2}. The total widths are about $1\,\text{GeV}$ with a partial width to all fermion pairs, $f\bar{f}$, of about $30\,\text{MeV}$. At $M_V = 100\,\text{GeV}$, the width of a 200 (220) GeV ω_T to $\gamma\pi_T$ is 300 (560) MeV and its (M_V-independent) width to $f\bar{f}$ is $45\,\text{MeV}$. The rapid fall of $\Gamma(\omega_T)$ with M_V is apparent. At $M_V = 300\,\text{GeV}$, the ω_T's branching fraction to $f\bar{f}$ is already 55%. [7]

---

[7]These decay rates are calculated from the formulas of Section 2. They ignore the

In Fig. 2 we show the total $\gamma\pi_T$ production rate ($\gamma\pi_T^0$, $\gamma\pi_T^{0\prime}$, and $\gamma\pi_T^{\pm}$) as a function of M_V for various M_{ω_T}. Again, the rapid fall with increasing M_V is apparent, with the cross sections dropping from 5 pb to 1 pb. The dependence on the input ρ_T–ω_T mass difference is not significant over the range we considered. Due to the additional $\gamma\pi_T$ channels, this rate at $M_V = 100$ GeV is twice what we found in Ref. [8] where we considered only $\omega_T \rightarrow \gamma\pi_T^0$. Note that our calculations are done in lowest order QCD with EHLQ Set 1 parton distribution functions [15]. For these Drell-Yan processes, next-order corrections to the cross sections and the distribution functions would increase the rates by about 50% ($K \simeq 1.5$). Thus, assuming that π_T^0 and $\pi_T^{0\prime}$ decay mainly to $b\bar{b}$ and π_T^+ to $c\bar{b}$, we expect that Run II searches for γ plus two jets with a single b-tag can cover the range $|Q_U + Q_D| \lesssim 1$ up to $M_{V_T} \simeq 350$ GeV. It is also important to look for the $\pi_T^{0\prime}$ in its two-gluon decay mode. It is an open question whether this could be seen above the γ plus two untagged jets background for, say, $B(\pi_T^0 \rightarrow gg) = 0.5$.

Figure 3 shows the $W\pi_T$ and $Z\pi_T$ production rates. [8] The $W\pi_T$ cross sections add up to 4–5 pb without the K-factor, for all the inputs of this case. This is about the same found in Ref. [8] even though there has been a doubling of the $\gamma\pi_T$ rate for $M_V = 100$ GeV. The reason for this is the new contribution from the transversely polarized $W_T\pi_T$ mode; see Eq.(11) and Table 1. We expect that, so long as $M_{\rho_T} \gtrsim M_W + M_{\pi_T}$, the process $\rho_T \rightarrow W\pi_T$ could be observed up to $M_{\rho_T} \simeq 400$ GeV in Run II. Unless there is substantial π_T^0–$\pi_T^{0\prime}$ mixing, very little of the $W\pi_T$ rate involves the isosinglet $\pi_T^{0\prime}$. To test for this mixing, one can look for $\pi_T^{0\prime} \rightarrow gg$ in association with a W. Such a signal should be discernible above background if the cross section is a few picobarns [16].

The $Z\pi_T$ rate is only about 0.9 pb for $M_{\rho_T} = 210$ GeV, about 50% less than we found in the simple model employed in Ref. [8]. If the ρ_T and π_T are discovered in any of their larger-rate channels, it would be interesting to confirm them here. At this cross section, it may just be possible to detect $\ell^+\ell^- jj$ with a b-tag in 2 fb^{-1} of data. Another interesting and challenging signature is $\not{E}_T$ plus two jets with a b-tag arising from $Z\pi_T \rightarrow \nu\bar{\nu}bj$.

effects of mixing, which are not entirely negligible for ρ_T^0 and ω_T. Nevertheless, they give a fair estimate of the relative contributions of the resonances to individual final state production rates.

[8] The $W_L W_L$ and $W_L Z_L$ cross sections, suppressed by $\sin^4\chi$, are less than 0.5 pb, not large enough to see above the standard model backgrounds.

Finally, we also show in Fig. 3 the total $\pi_T\pi_T$ cross section for $M_{\rho_T} = 210\,\mathrm{GeV}$ and $M_{\pi_T} = 110\,\mathrm{GeV}$. This continuum production rate is only $0.12\,\mathrm{pb}$. Even with very efficient b-identification, it seems unlikely that it will be possible to detect technipions in this mode above the four-jet background.

Technivector decays to lepton pairs may be an accessible signature at the Tevatron. Figures 4 and 5 show the mass distribution, $d\sigma(p\bar{p} \to e^+e^-)/d\sqrt{\hat{s}}$, for the extreme cases $M_V = 100$ and $500\,\mathrm{GeV}$. The input ρ_T–ω_T mass splittings in each figure are zero and $\pm 10\,\mathrm{GeV}$. From this, one can judge the effect of mixing. For all M_V, most of the signal comes from the ω_T because it is proportional to $(Q_U + Q_D)^2 = 25/9$ and its branching ratio to e^+e^- is several times larger than the ρ_T^0's. The signal-plus-background rates for $M_V = 100\,\mathrm{GeV}$, integrated over the entire resonance region from 195 to $225\,\mathrm{GeV}$, are 0.19, 0.17, and $0.15\,\mathrm{pb}$ for $M_{\omega_T} = 200$, 210, and $220\,\mathrm{GeV}$, while the standard-model background is $0.13\,\mathrm{pb}$. For $M_V = 500\,\mathrm{GeV}$, the branching ratio of ω_T to e^+e^- increases by a factor of 7 and the total e^+e^- rate doubles to 0.38, 0.30, and $0.31\,\mathrm{pb}$. No smearing due to detector resolution was included here. The separated resonances are just at or below the detectors' dielectron mass resolutions. It will be interesting to see what these mass distributions look like when the effects of a real detector are included [17].

There is no observable $\rho_T^\pm$ enhancement in the $\ell^\pm\nu_\ell$ cross section. This is clear from the (theoretical) invariant mass distributions of Fig. 6. The signal rate is small because $B(\rho_T^\pm \to \ell^\pm\nu_\ell)$ is. This is true for all the input parameters we considered.

Case 2: $M_{\pi_T} = 110\,\mathrm{GeV}$; $Q_U + Q_D = 0$

The sharp decrease in the $\omega_T \to \gamma\pi_T$ and e^+e^- rates when $Q_U + Q_D = 0$ is apparent in Figs. 7–9. Because most of the $\gamma\pi_T$ cross section in case 1 come from ω_T production, it has in this case fallen by a factor of 20–50, depending on M_V. The e^+e^- signal rate is tiny because it all comes from ρ_T^0. Finally, because ω_T mixing with γ and Z vanishes when $Q_U + Q_D = 0$ (see Eq. (19)), so does ρ_T–ω_T mixing, and all the production rates are independent of M_{ω_T}. The $W\pi_T$ cross section is still large, about $4\,\mathrm{pb}$, and represents the best way to discover ρ_T and π_T in this extreme case. The $\pi_T\pi_T$ rate is still about $0.12\,\mathrm{pb}$.

Case 3: $M_{\pi_T} = 100\,\mathrm{GeV}$; $Q_U + Q_D = 5/3$

Now, the ρ_T is just above threshold to decay into a pair of technipions.

The ρ_T widths have increased to 2–3 GeV; see Fig. 10. This has caused a 25% decrease in the $\gamma\pi_T$ rates compared to case 1 (Fig. 11), but this signal is still a relatively easy one in Run II up to $M_{\omega_T} \simeq 350$ GeV. Figure 12 shows the $W\pi_T$, $Z\pi_T$ and $\pi_T\pi_T$ cross sections versus M_V. The $W\pi_T$ rate is 3 pb, still large enough to detect, and $\sigma(Z\pi_T) = 0.5$–1.0 pb, as before. We still expect that $\rho_T \to W\pi_T$ could be detected in Run II up to $M_{\rho_T} \simeq 400$ GeV so long as $M_{\rho_T} \gtrsim M_W + M_{\pi_T}$. The $\pi_T\pi_T$ rate has grown a factor of 20–30 to 2.5–4 pb because it is unsuppressed by powers of $\sin\chi$. Roughly half this is $\pi_T^+\pi_T^- \to c\bar{b}b\bar{c}$ and half is $\pi_T^\pm\pi_T^0 \to c\bar{b}b\bar{b}$. It should be possible to see such signals at rates this large in Run II. The ultimate mass reaches for $\rho_T \to \pi_T\pi_T$ in Run II and in the proposed 20–30 fb^{-1} Run III remain to be determined by detailed simulations. Finally, as we see in Figs. 13 and 14, the e^+e^- rates again are due mainly to ω_T production and little affected by the lowered π_T mass. Integrated over the resonance region, they are very similar to those found in case 1: signal-plus-background rates of 0.18, 0.16, and 0.14 pb over a background of 0.13 pb for $M_V = 100$ GeV; they are 0.36, 0.24, and 0.29 pb for $M_V = 500$ GeV.

5 Concluding Remarks

The straw-man model studied in this paper assumes a relatively uncluttered, minimal spectrum for low-scale technicolor. We believe that the parameters chosen for study are sufficiently generic to warrant our expectation that, up to $M_{\rho_T} \simeq 400$ GeV, such a spectrum can be ruled out—or established—in Run II at the Tevatron. A richer and more complicated spectrum, due to several low-lying technifermion doublets might be more representative of low-scale technicolor and might be more (or less) difficult to pin down experimentally. One generalization of the TCSM would include a minimal set of $SU(3)$-triplet technifermion doublets. We plan to carry it out in the near future. Together with the color-singlet states discussed here, that would make for a very rich experimental program in technicolor, even into the proposed Tevatron Run III.

6 Acknowledgements

References

[1] B. Holdom, Phys. Rev. **D24**, 1441 (1981); Phys. Lett. **150B**, 301 (1985); T. Appelquist, D. Karabali and L. C. R. Wijewardhana, Phys. Rev. Lett. **57**, 957 (1986); T. Appelquist and L. C. R. Wijewardhana, Phys. Rev. **D36**, 568 (1987); K. Yamawaki, M. Bando and K. Matumoto, Phys. Rev. Lett. **56**, 1335 (1986); T. Akiba and T. Yanagida, Phys. Lett. **169B**, 432 (1986).

[2] Y. Nambu, in *New Theories in Physics*, Proceedings of the XI International Symposium on Elementary Particle Physics, Kazimierz, Poland, 1988, edited by Z. Adjuk, S. Pokorski and A. Trautmann (World Scientific, Singapore, 1989); Enrico Fermi Institute Report EFI 89-08 (unpublished); V. A. Miransky, M. Tanabashi and K. Yamawaki, Phys. Lett. **221B**, 177 (1989); Mod. Phys. Lett. **A4**, 1043 (1989); W. A. Bardeen, C. T. Hill and M. Lindner, Phys. Rev. **D41**, 1647 (1990). C. T. Hill, Phys. Lett. **266B**, 419 (1991) ; S. P. Martin, Phys. Rev. **D45**, 4283 (1992); *ibid* **D46**, 2197 (1992); Nucl. Phys. **B398**, 359 (1993); M. Lindner and D. Ross, Nucl. Phys. **B370**, 30 (1992); R. Bönisch, Phys. Lett. **268B**, 394 (1991); C. T. Hill, D. Kennedy, T. Onogi, H. L. Yu, Phys. Rev. **D47**, 2940 (1993).

[3] C. T. Hill, Phys. Lett. **345B**, 483 (1995).

[4] K. Lane and E. Eichten, Phys. Lett. **B352**, 382 (1995) ; K. Lane, Phys. Rev. **D54**, 2204 (1996); K. Lane, Phys. Lett. **B433**, 96 (1998).

[5] S. Weinberg, Phys. Rev. **D19**, 1277 (1979); L. Susskind, Phys. Rev. **D20**, 2619 (1979).

[6] E. Eichten and K. Lane, Phys. Lett. **B90**, 125 (1980).

[7] K. Lane and E. Eichten, Phys. Lett. **B222**, 274 (1989); K. Lane and M. V. Ramana, Phys. Rev. **D44**, 2678 (1991).

[8] E. Eichten and K. Lane, Phys. Lett. **B388**, 803 (1996); E. Eichten, K. Lane and J. Womersley, Phys. Lett. **B405**, 305 (1997); E. Eichten, K. Lane and J. Womersley, Phys. Rev. Lett. **80**, 5489 (1998).

[9] *Search for Technicolor Particles in W + 2 jet with b-tag Channel at CDF*, T. Handa, K. Maeshima, J. Valls, R. Vilar, The CDF Collaboration, FERMILAB-CONF-98/016-E, published in Proceedings of Workshop on Physics at the First Muon Collider and at the Front End of a Muon Collider, Fermi National Accelerator Laboratory, Batavia, IL, November 6-9, 1997.

[10] *Search for a Technicolor ω_T Particle in Events with a Photon and a b-quark Jet at CDF*, F. Abe et al., The CDF Collaboration, Fermilab-PUB-98/321-E, submitted to Physical Review Letters, October 1998.

[11] *CDF Searches for New Phenomena.*, D. Toback, The CDF Collaboration, FERMILAB-CONF-98/183-E, published in Proceedings 12th Les Rencontres de Physique de la Vallee D'Aosta: Results and Perspectives in Particle Physics, La Thuile, Italy, March 1-7, 1998;
Searches for Exotic Particles at the Tevatron. C. Grosso-Pilcher, The CDF Collaboration, FERMILAB-CONF-98/306-E. Published Proceedings 29th International Conference on High Energy Physics (ICHEP 98), Vancouver, British Columbia, Canada, July 23-29, 1998.

[12] K. Lane, *Technicolor Production and Decay Rates in the Technicolor Straw Man Model*, hep-ph/9903372, Boston University Preprint BUHEP-99-5, March 1999.

[13] S. Mrenna and J. Womersley, private communication.

[14] T. Sjöstrand, Comp. Phys. Com. **82**, 74 (1994).

[15] E. Eichten, I. Hinchliffe, K. Lane and C. Quigg, Rev. Mod. Phys **56**, 579 (1984).

[16] S. Mrenna and J. Womersley, *Can a light technipion be discovered at the Tevatron if it decays to two gluons?*, to be published in Physics Letters B, hep-ph/9901202, Fermilab-PUB-99-002 (1999).

[17] M. Narain, private communication.
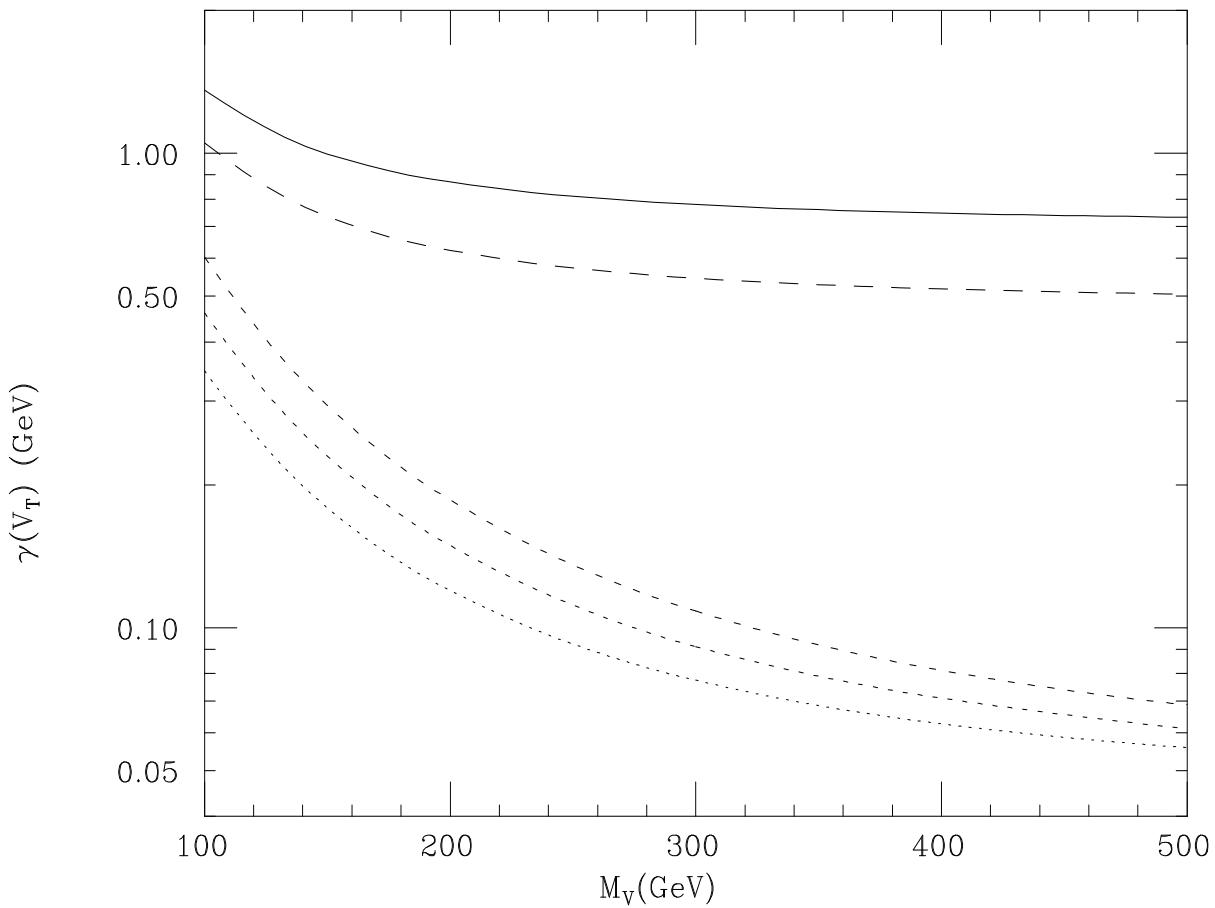
Figure 1: Technivector meson decay rates versus $M_V = M_A$ for ρ_T^0 (solid curve) and $\rho_T^\pm$ (long-dashed) with $M_{\rho_T} = 210\,\text{GeV}$, and ω_T with $M_{\omega_T} = 200$ (lower dotted), 210 (lower short-dashed), and 220 GeV (lower medium-dashed); $Q_U + Q_D = 5/3$ and $M_{\pi_T} = 110\,\text{GeV}$.
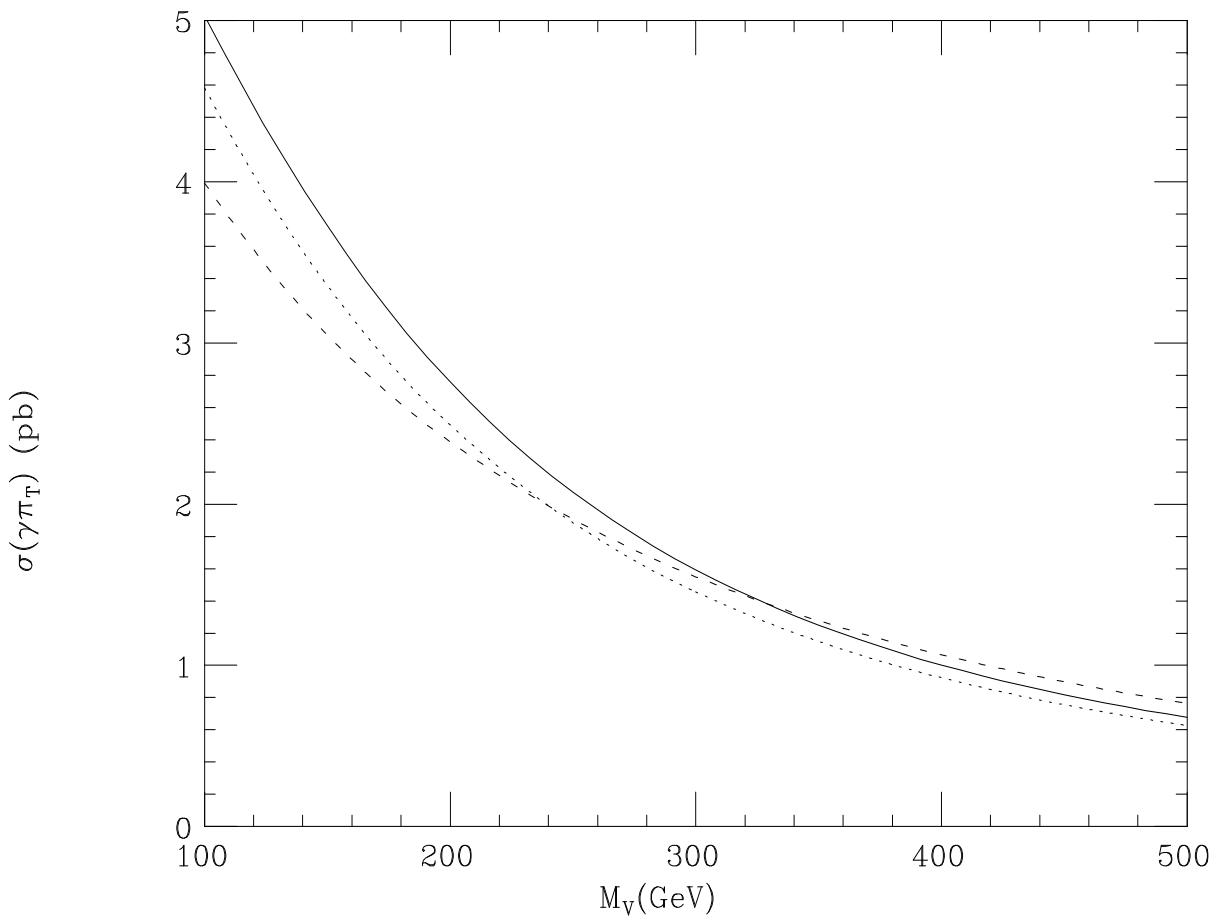
Figure 2: Production rates in $p\bar{p}$ collisions at $\sqrt{s} = 2\,\mathrm{TeV}$ for the sum of ω_T, ρ_T^0, $\rho_T^\pm \to \gamma\pi_T$ versus M_V, for $M_{\rho_T} = 210\,\mathrm{GeV}$ and $M_{\omega_T} = 200$ (dotted curve), 210 (solid), and $220\,\mathrm{GeV}$ (short-dashed); $Q_U + Q_D = 5/3$, and $M_{\pi_T} = 110\,\mathrm{GeV}$.
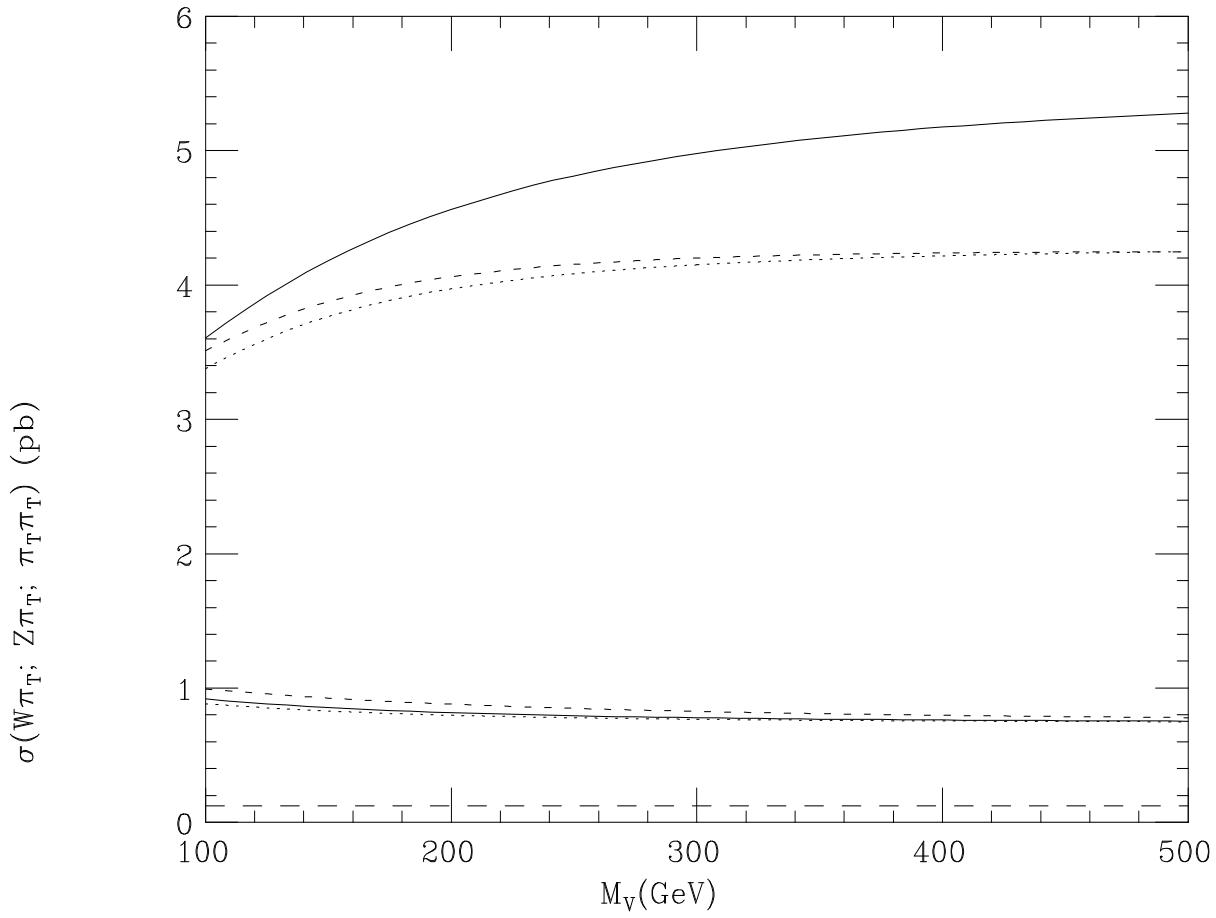
Figure 3: Production rates for ω_T, ρ_T^0, $\rho_T^\pm \to W\pi_T$ (upper curves) and $Z\pi_T$ (lower curves) versus M_V, for $M_{\rho_T} = 210\,\mathrm{GeV}$ and $M_{\omega_T} = 200$ (dotted curve), 210 (solid), and 220 GeV (short-dashed); $Q_U + Q_D = 5/3$ and $M_{\pi_T} = 110\,\mathrm{GeV}$. Also shown is $\sigma(\rho_T \to \pi_T\pi_T)$ (lowest dashed curve).
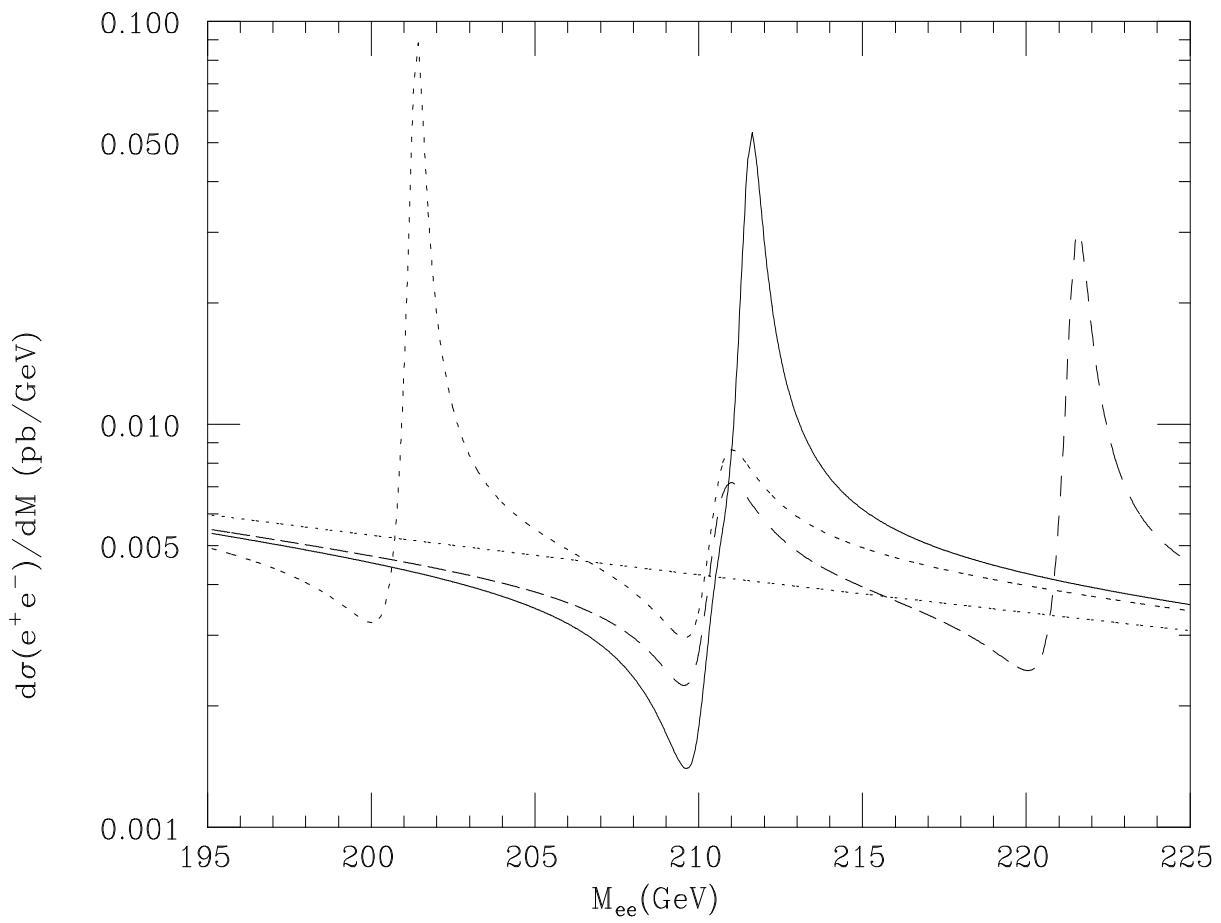
Figure 4: Invariant mass distributions for ω_T, $\rho_T^0 \to e^+e^-$ for $M_{\rho_T} = 210\,\text{GeV}$ and $M_{\omega_T} = 200$ (short-dashed curve), 210 (solid), and 220 GeV (long-dashed); $M_V = 100\,\text{GeV}$. The standard model background is the sloping dotted line. $Q_U + Q_D = 5/3$ and $M_{\pi_T} = 110\,\text{GeV}$.
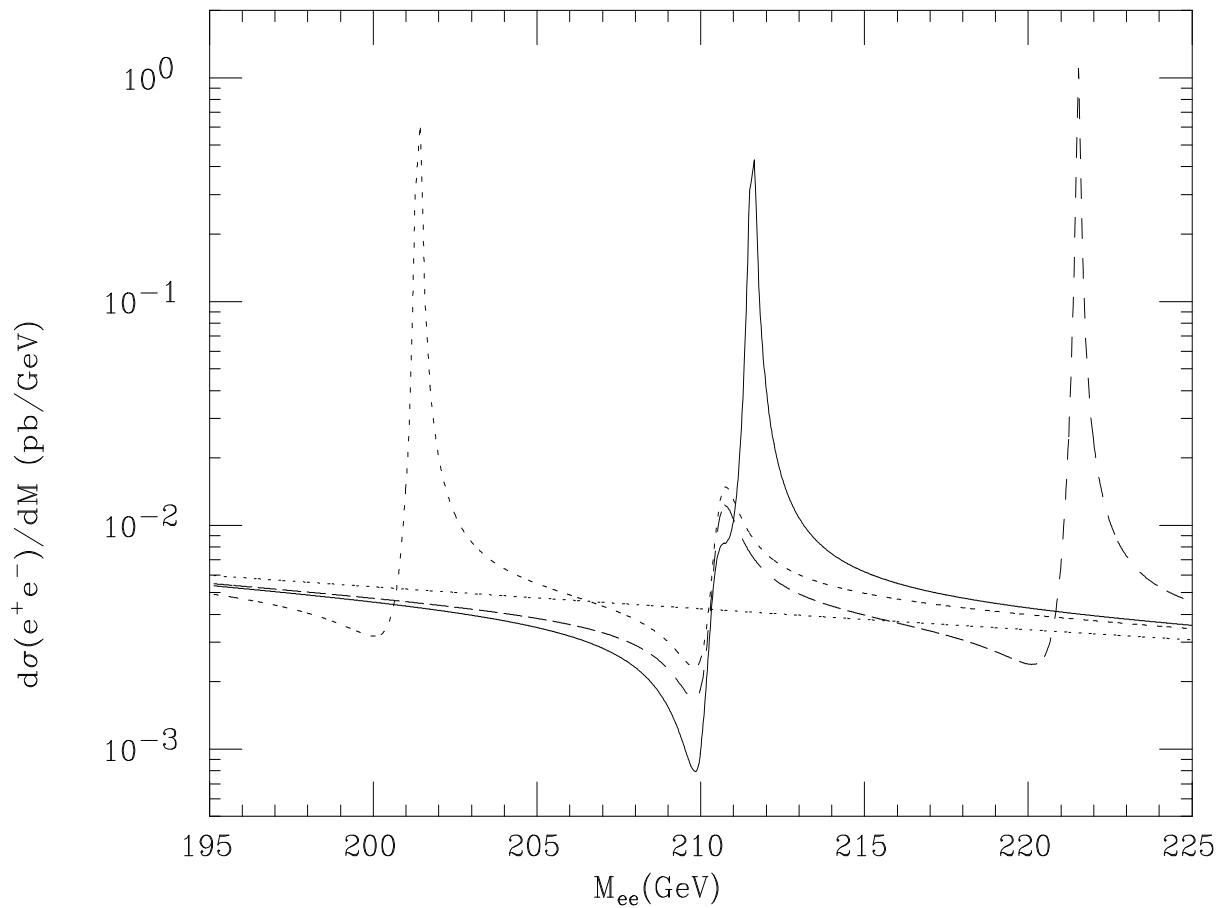
Figure 5: Invariant mass distributions for ω_T, $\rho_T^0 \to e^+e^-$ for $M_{\rho_T} = 210\,\mathrm{GeV}$ and $M_{\omega_T} = 200$ (short-dashed curve), 210 (solid), and 220 GeV (long-dashed); $M_V = 500\,\mathrm{GeV}$. The standard model background is the sloping dotted line. $Q_U + Q_D = 5/3$ and $M_{\pi_T} = 110\,\mathrm{GeV}$.
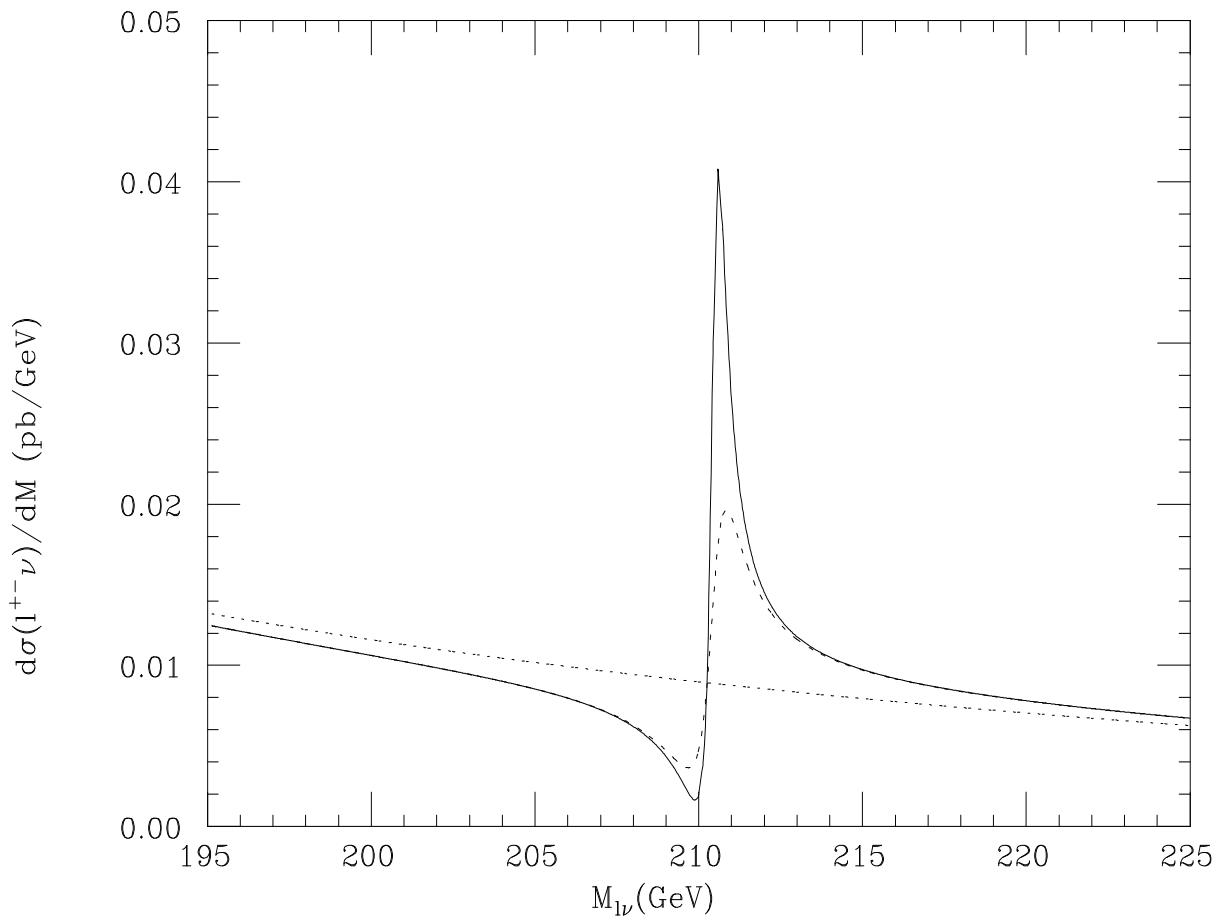
Figure 6: Invariant mass distributions for $\rho_T^{\pm} \to \ell^{\pm}\nu$ for $M_{\rho_T} = 210\,\text{GeV}$ and $M_V = 100\,\text{GeV}$ (dashed curve) and $500\,\text{GeV}$ (solid); The standard model background is the sloping dotted line. $Q_U + Q_D = 5/3$ and $M_{\pi_T} = 110\,\text{GeV}$.
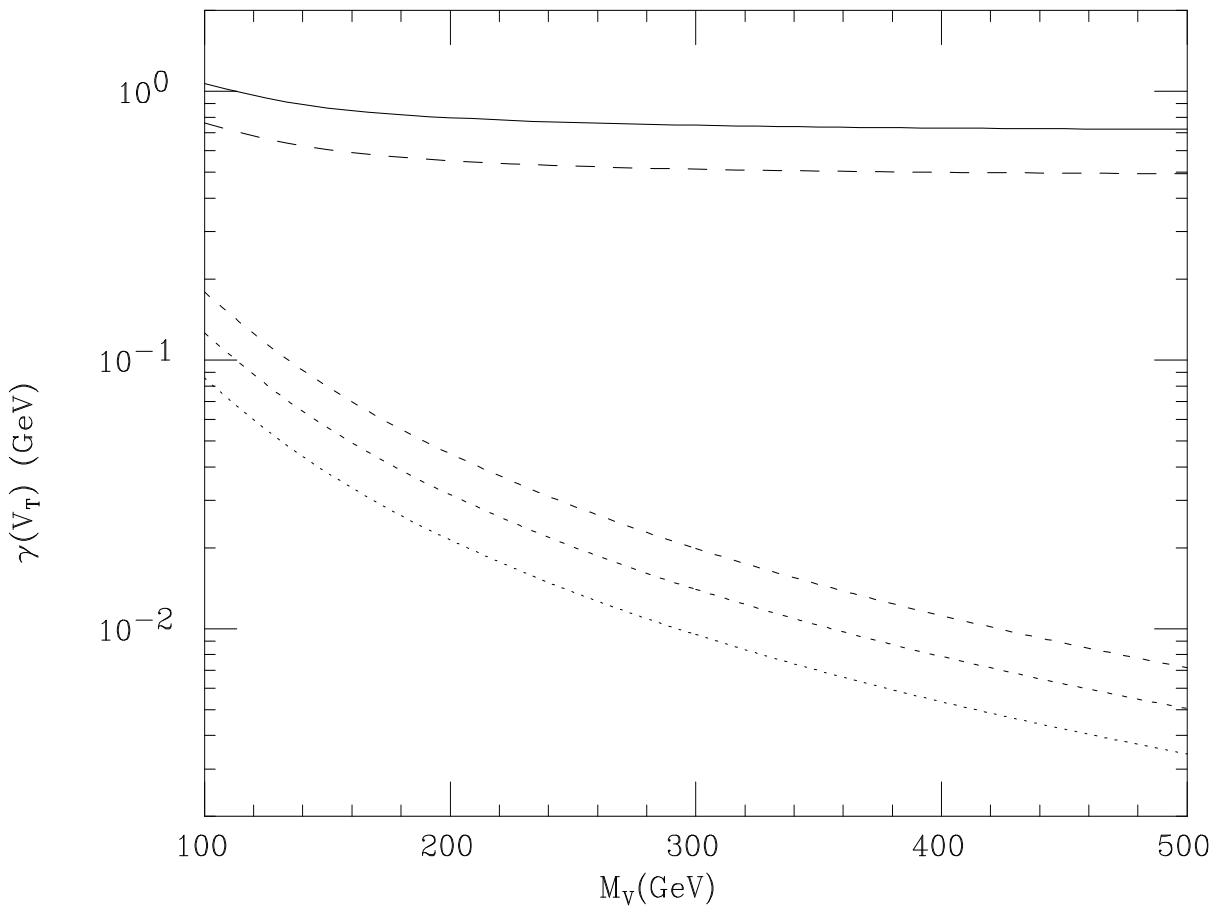
Figure 7: Technivector meson decay rates versus $M_V = M_A$ for ρ_T^0 (solid curve) and $\rho_T^\pm$ (long-dashed) with $M_{\rho_T} = 210\,\text{GeV}$, and ω_T with $M_{\omega_T} = 200$ (lower dotted), 210 (lower short-dashed), and $220\,\text{GeV}$ (lower medium-dashed); $Q_U + Q_D = 0$ and $M_{\pi_T} = 110\,\text{GeV}$.
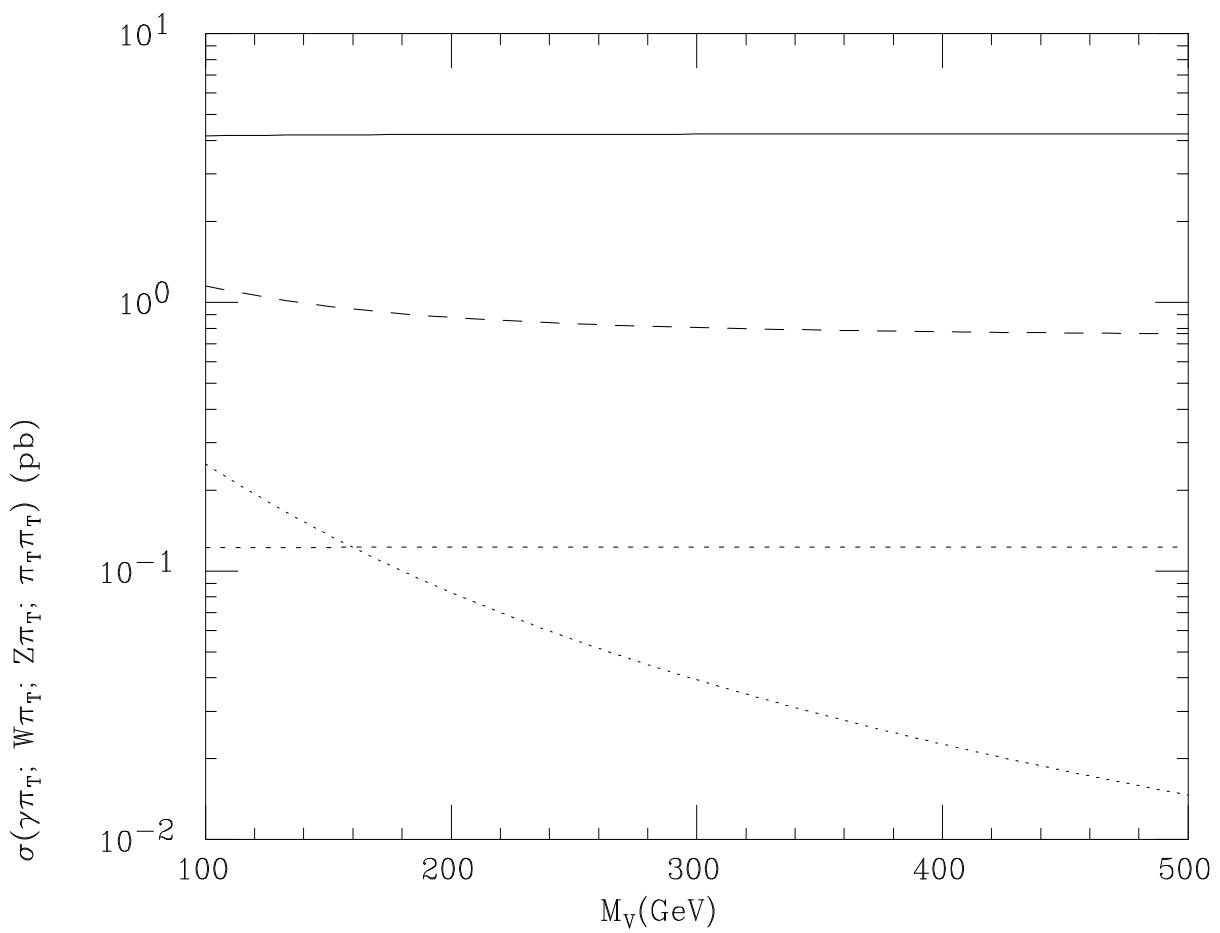
Figure 8: Production rates for ω_T, ρ_T^0, $\rho_T^\pm \rightarrow W\pi_T$ (solid curve), $Z\pi_T$ (long-dashed), $\pi_T\pi_T$ (short-dashed) and $\gamma\pi_T$ (dotted) versus M_V, for $M_{\rho_T} = 210\,\mathrm{GeV}$ and $M_{\omega_T} = 200\text{–}220\,\mathrm{GeV}$; $Q_U + Q_D = 0$ and $M_{\pi_T} = 110\,\mathrm{GeV}$.
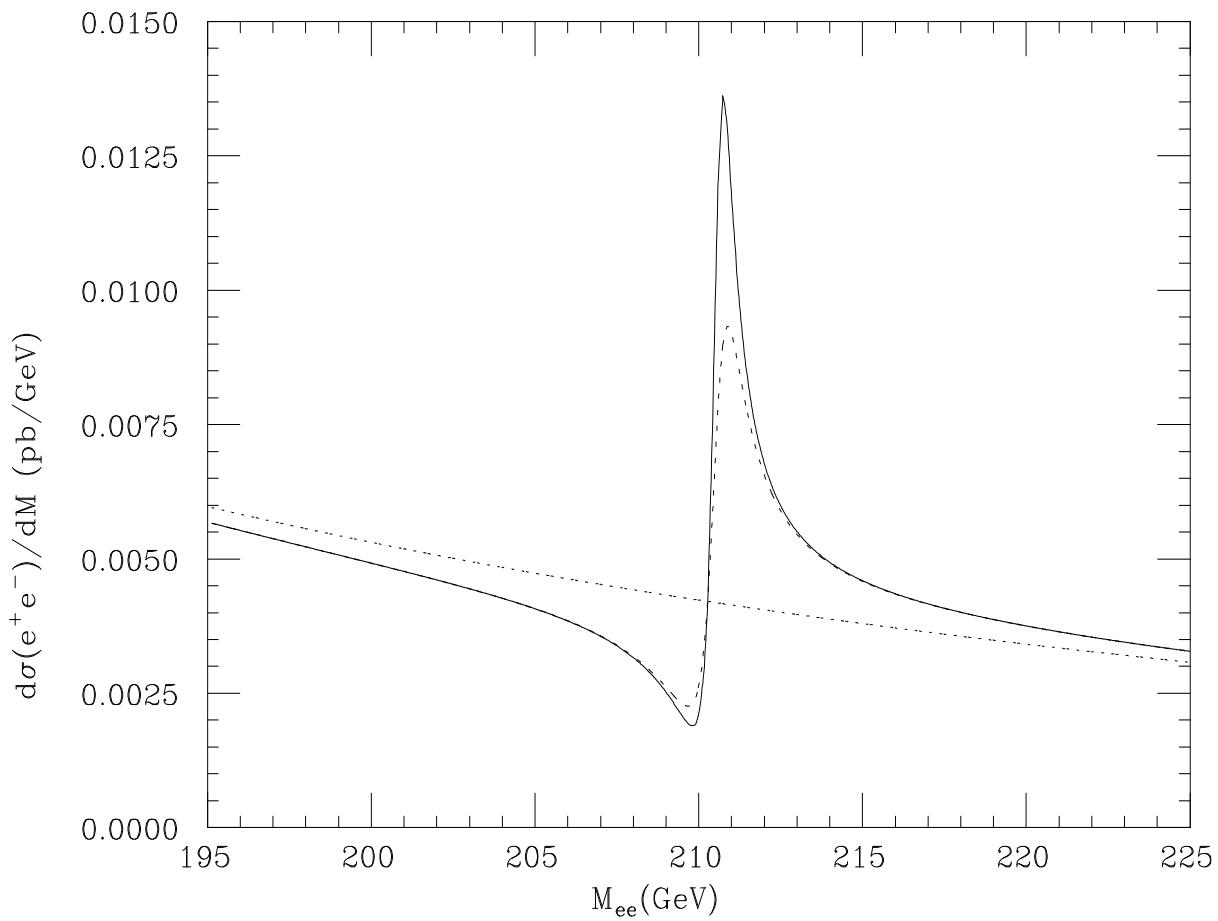
Figure 9: Invariant mass distributions for $\rho_T^0 \to e^+e^-$ for $M_{\rho_T} = 210\,\text{GeV}$; $M_V = 100\,\text{GeV}$ (dashed curve) and $500\,\text{GeV}$ (solid). The standard model background is the sloping dotted line. $Q_U + Q_D = 0$ and $M_{\pi_T} = 110\,\text{GeV}$.
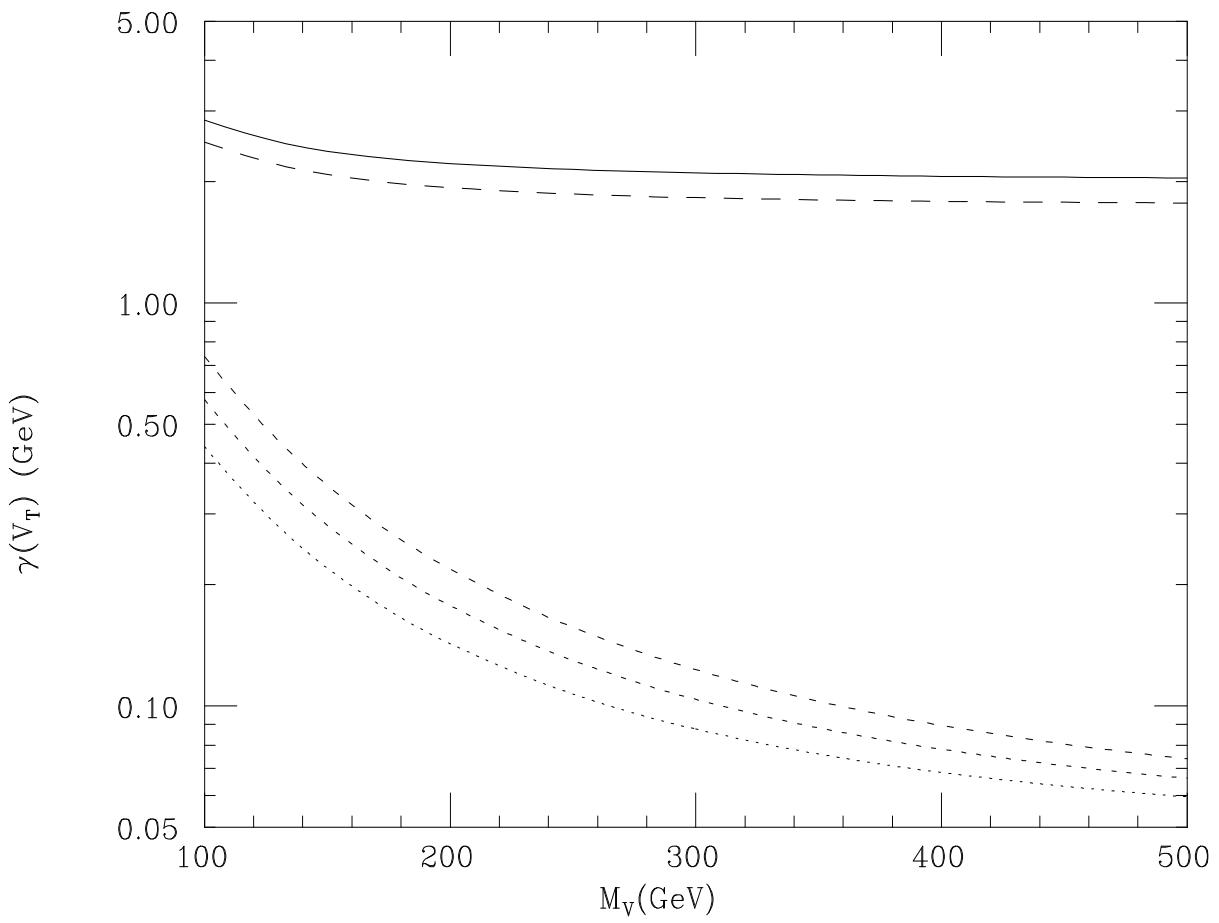
Figure 10: Technivector meson decay rates versus $M_V = M_A$ for ρ_T^0 (solid curve) and $\rho_T^{\pm}$ (long-dashed) with $M_{\rho_T} = 210\,\mathrm{GeV}$, and ω_T with $M_{\omega_T} = 200$ (lower dotted), 210 (lower short-dashed), and 220 GeV (lower medium-dashed); $Q_U + Q_D = 5/3$ and $M_{\pi_T} = 100\,\mathrm{GeV}$.
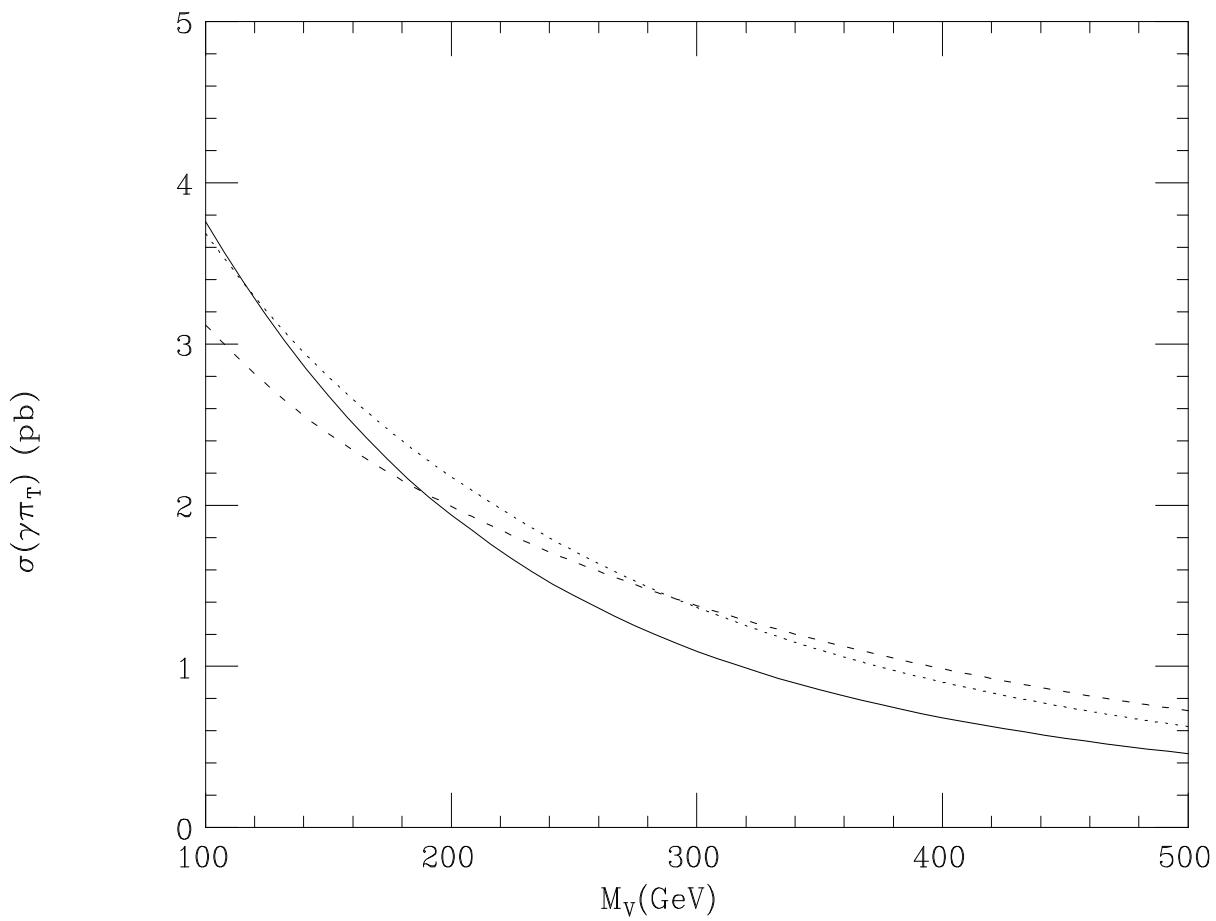
Figure 11: Production rates for the sum of ω_T, ρ_T^0, $\rho_T^\pm \to \gamma\pi_T$ versus M_V, for $M_{\rho_T} = 210\,\mathrm{GeV}$ and $M_{\omega_T} = 200$ (dotted curve), 210 (solid), and 220 GeV (short-dashed); $Q_U + Q_D = 5/3$, and $M_{\pi_T} = 100\,\mathrm{GeV}$.
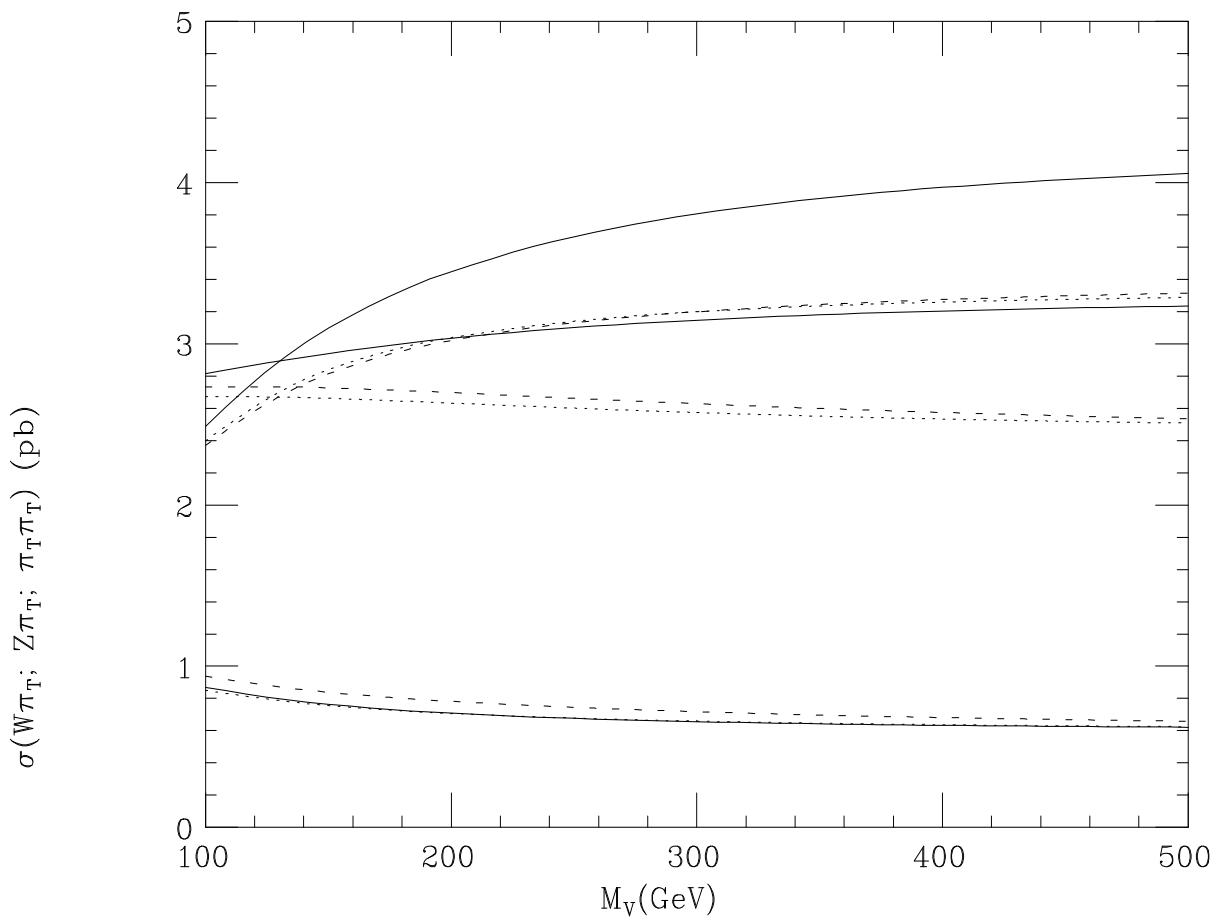
Figure 12: Production rates for ρ_T^0, $\rho_T^{\pm}$, $\omega_T \to \pi_T\pi_T$ (upper three curves), $W\pi_T$ (middle three curves), and $Z\pi_T$ (lower curves) versus M_V, for $M_{\rho_T} = 210\,\text{GeV}$ and $M_{\omega_T} = 200$ (dotted), 210 (dashed), and 220 GeV (solid); $Q_U + Q_D = 5/3$ and $M_{\pi_T} = 100\,\text{GeV}$.
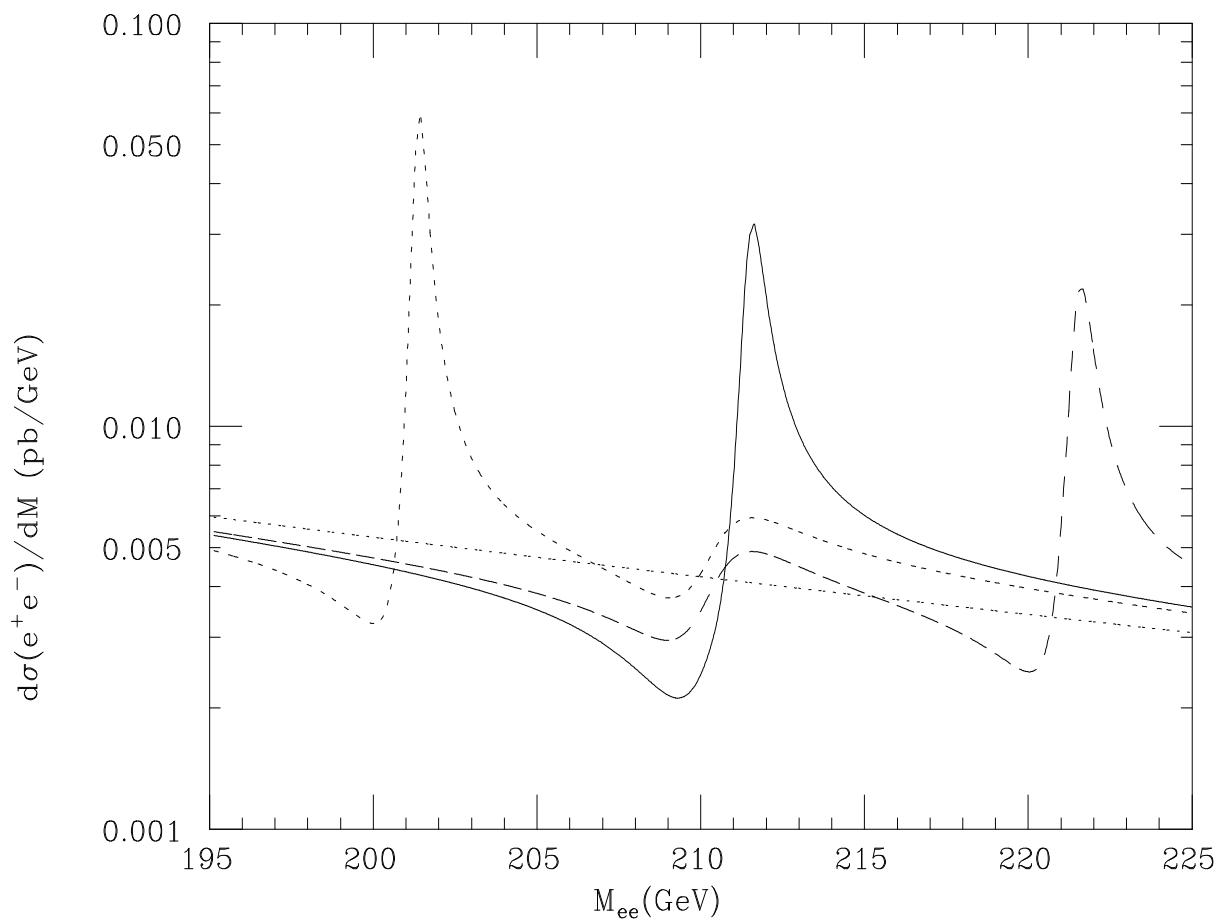
Figure 13: Invariant mass distributions for ω_T, $\rho_T^0 \rightarrow e^+ e^-$ for $M_{\rho_T} = 210\,\text{GeV}$ and $M_{\omega_T} = 200$ (short-dashed curve), 210 (solid), and 220 GeV (long-dashed); $M_V = 100\,\text{GeV}$. The standard model background is the sloping dotted line. $Q_U + Q_D = 5/3$ and $M_{\pi_T} = 100\,\text{GeV}$.
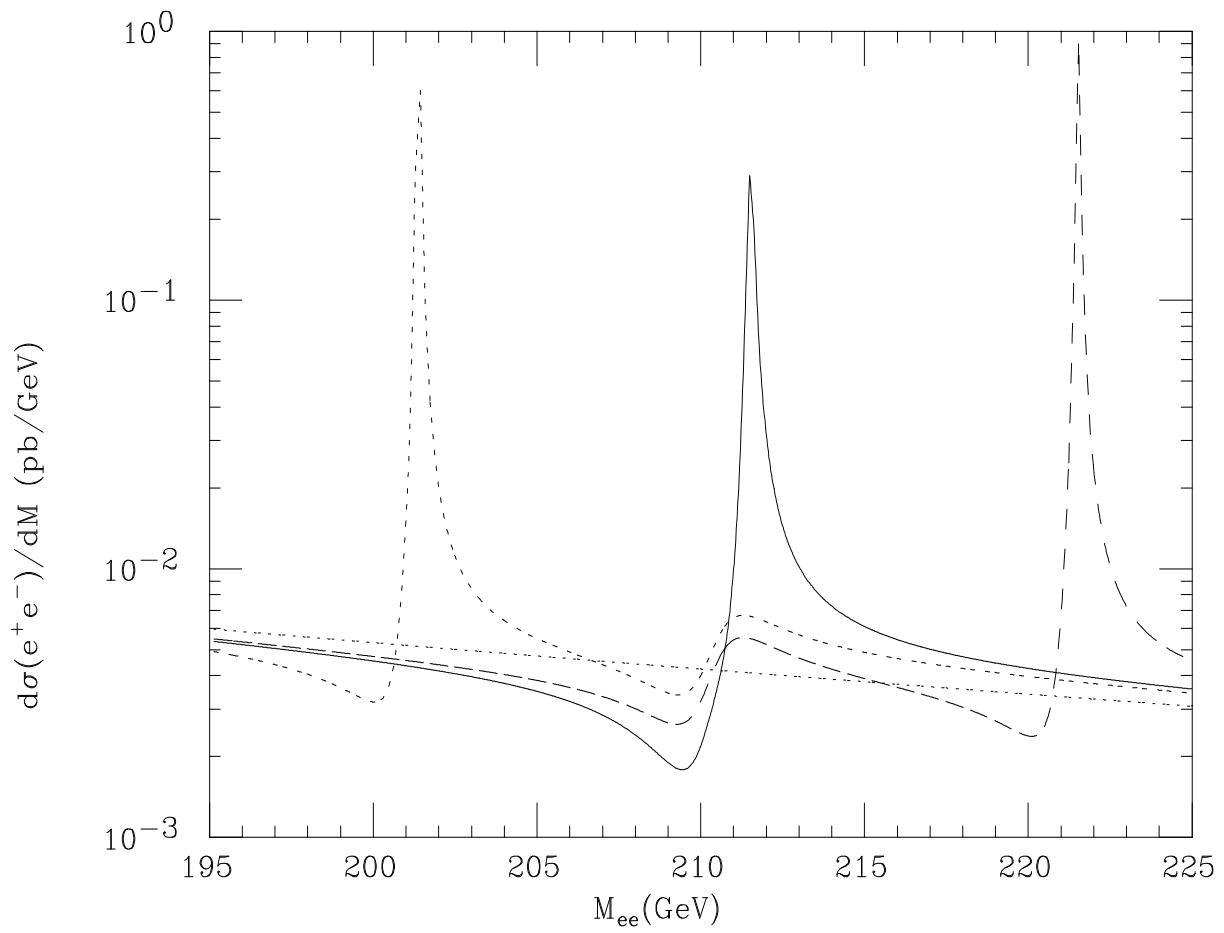
Figure 14: Invariant mass distributions for ω_T, $\rho_T^0 \rightarrow e^+e^-$ for $M_{\rho_T} = 210\,\mathrm{GeV}$ and $M_{\omega_T} = 200$ (short-dashed curve), 210 (solid), and 220 GeV (long-dashed); $M_V = 500\,\mathrm{GeV}$. The standard model background is the sloping dotted line. $Q_U + Q_D = 5/3$ and $M_{\pi_T} = 100\,\mathrm{GeV}$.